Available online at www.sciencedirect.com
ScienceDirect
Ultramicroscopy 107 (2007) 604–609
ultramicroscopy
www.elsevier.com/locate/ultramic

Simulation of partially coherent image formation in a compact soft X-ray microscope

Olov von Hofsten*, Per A.C. Takman, Ulrich Vogt

Biomedical and X-ray Physics, Department of Applied Physics, Royal Institute of Technology/Albanova, SE-106 91 Stockholm, Sweden

Received 7 September 2006; received in revised form 29 November 2006; accepted 6 December 2006

Abstract

In this paper, we describe a numerical method of simulating two-dimensional images in a compact soft X-ray microscope using partially coherent illumination considerations. The work was motivated by recent test object images obtained by the latest generation in-house compact soft X-ray microscope, which showed diffraction-like artifacts not observed previously. The numerical model approximates the condenser zone plate as a secondary incoherent source represented by individually coherent but mutually incoherent source points, each giving rise to a separate image. A final image is obtained by adding up all the individual source point contributions. The results are compared with the microscope images and show qualitative agreement, indicating that the observed effects are caused by partially coherent illumination.

PACS: 7.85.Tt; 42.30.Kq; 42.30.Va; 42.79.Ci

Keywords: X-ray microscopy; Partial coherence; Image formation; Zone plates

1. Introduction

Transmission X-ray microscopy is an established technique for imaging of samples with sub-30-nm resolution [1]. A prominent spectral region for X-ray microscopy is the so-called water-window defined by the K-absorption edges of oxygen and carbon (2.3–4.4 nm) in which water has a relative transparency against carbon containing materials. Thus a natural contrast is provided for biological material in a 10 μm layer of water, the thickness of a typical cell. The possibility of high-resolution biological imaging of relatively thick samples is a major advantage of X-ray microscopy and distinguishes this method from other high-resolution techniques like electron or atomic force microscopy. In addition, X-ray microscopy combined with tomographic techniques can create three-dimensional images of biological [2] or soil samples [3] with nanometer scale resolution.

The optical arrangement of a transmission X-ray microscope is similar to its visible light counterpart and consists of condenser optic for object illumination and objective optic to create a high-resolution image. A number of instruments can be found at storage ring facilities using synchrotron radiation as light source [1]. In addition, the Biomedical and X-ray Physics (BIOX) group has pioneered the development of compact X-ray microscopes [4,5], enabling laboratory operation of these instruments [6,7] in order to overcome the limited accessibility of synchrotron-based microscopes. In the present publication, we present a numerical method for the simulation of two-dimensional X-ray microscope images obtained with partially coherent object illumination. While this condition is found in all transmission X-ray microscopes, it is especially important for compact microscopes using zone plate condensers because of the numerical aperture mismatch between condenser and objective.

The image formation process in a normal transmission microscope, working either with coherent or incoherent object illumination, is readily described using Fourier optical methods [8] and can easily be implemented

*Corresponding author.
E-mail address: olov.hofsten@biox.kth.se (O. von Hofsten).

0304-3991/$ - see front matter © 2007 Elsevier B.V. All rights reserved.
doi:10.1016/j.ultramic.2006.12.001

numerically. However, the situation changes if the object illumination is partially coherent. While an analytical solution to the problem exists in the form of a four-fold integral [9], the numerical implementation is more complicated. The program SPLAT [10,11] is a numerical tool for imaging simulations including partial coherence and is based on the Hopkins theory of partial coherence. It was developed for optical lithography applications and solves the four-fold integral numerically. Although SPLAT has the ability to simulate full two-dimensional images, most X-ray microscopy investigations have so far been restricted to one dimension. SPLAT was applied to investigate the influence of partial coherence in a soft X-ray transmission microscope on the response of a one-dimensional knife edge object [12,13] and to calculate the theoretical resolution of the X-ray microscope at the Advanced Light source in Berkeley [14]. Other publications investigated dark field X-ray microscopy [15] and cryo X-ray microscopy [16] with other numerical models taking partial coherence into account, but again the calculations were limited to one-dimensional objects.

We have developed a program that can simulate a complete two-dimensional X-ray microscope image including partially coherent object illumination. The model is based on a Fourier-optics approach and requires primarily the calculation of Fourier transforms. Thereby, the model is easily implemented numerically using standard fast Fourier transform algorithms. The work was motivated by the fact that the latest generation of the compact soft X-ray microscope operated by the BIOX group uses a wavelength of 2.48 nm emitted by a liquid-nitrogen-jet laser-plasma source [4]. Due to this wavelength, a zone plate condenser must be used with a relatively low numerical aperture compared to the zone plate objective. This results in a partially coherent illumination of the object. Calculated test-object images could explain edge-effects visible in measured images that previously were not understood.

2. The compact soft X-ray microscope

Fig. 1 shows the basic arrangement of the compact soft X-ray microscope. A laser-produced plasma is used as a compact X-ray source utilizing a liquid-nitrogen-jet target. The plasma emits nitrogen line emission at $\lambda = 2.48$ nm, close to the normal operation wavelength of 2.4 nm for synchrotron-based water-window instruments. The achieved average X-ray flux is $\sim 1.0 \times 10^{12}$ photons/(pulse × sr × line) and the source size is ~ 20 μm full-width at half-maximum. Details on the source can be found in Ref. [17]. The source is imaged with a magnification of 1 by a nickel condenser zone plate into the object plane resulting in critical illumination conditions [18]. The condenser consists only of a ring with an outer diameter of 4.53 mm, a ring width of 376 μm and an outermost zone width of 49 nm [19]. The focal length in the first diffraction order is 90 mm at 2.48 nm, so the distance between condenser and object plane is 180 mm, resulting in a numerical aperture of $NA_{condenser} = 0.0127$. A pinhole close to the object plane in combination with a chromium filter in front of the condenser (not shown in Fig. 1) selects only the 2.48 nm emission line from the plasma. Therefore, the resulting monochromaticity is given by the line width itself, which is estimated to be $\lambda/\Delta\lambda > 500$ [20]. This is suitable for microscope operation and quasimonochromatic approximations will be used in the simulation described in the next paragraph. The object is followed by the zone plate objective, and for the present work a nickel zone plate with a diameter of 58 μm and an outermost zone width of 30 nm was used. The numerical aperture is $NA_{objective} = 0.0413$.

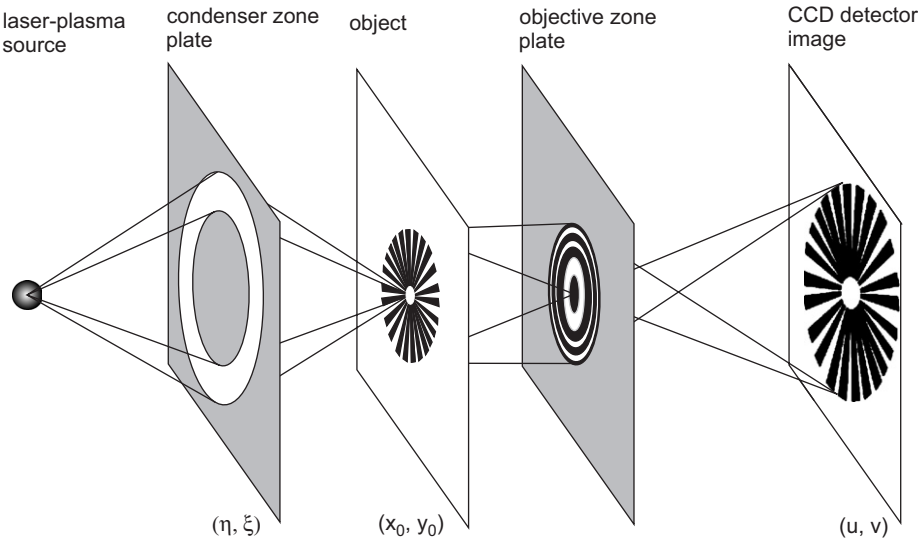

Fig. 1. The arrangement in the compact soft X-ray microscope. The condenser zone plate images the source into the object plane, providing critical illumination. An objective zone plate images the object onto an X-ray CCD detector. Note that sizes and distances are not to scale.

This objective has a focal length of 682 μm at 2.48 nm. The final image is recorded by an X-ray CCD-camera, and the magnification in the image was 1000×. More information on the zone plate fabrication can be found in Ref. [21] and on the microscope performance in Ref. [4].

Fig. 2 shows the image obtained for a Siemens star test object, made of 60–88 nm thick nickel. A Siemens star is a standard pattern for resolution tests in microscopy since it has varying spatial frequencies in all image directions. Due to fabrication issues, the central part of the star is missing. The image was taken with an exposure time of 5 min. A closer investigation of the image reveals diffraction-like edge effects which are clearly visible in the line plots in Fig. 2 taken at different radial position of the star. These effects were not seen in images taken by the previous microscope arrangement with a multilayer mirror condenser employing methanol-jet-target laser-plasma emission at 3.37 nm [22]. The question was raised whether this effect was the result of the partially coherent object illumination introduced by the relatively large mismatch in numerical aperture between the condenser and objective zone plates (which was not the case for the arrangement with the multilayer mirror condenser). The ratio between the numerical apertures yields the coherence factor m, which quantifies the degree of coherence in the microscope object plane. It is given by [23]

$$m = \frac{\mathrm{NA}_{\mathrm{condenser}}}{\mathrm{NA}_{\mathrm{objective}}}. \tag{2.1}$$

For the optics used, the coherence factor is $m = 0.3$, which clearly is in the partially coherent range, but closer to the coherent limit ($m = 0$) than to the standard case of matched apertures ($m = 1$) or the incoherent limit ($m \to \infty$). To understand the imaging process under the given conditions and to explain the experimentally obtained imaging results, a numerical simulation of the microscope including partially coherent object illumination was performed, as described in the next paragraph.

3. Theory

Our mathematical description of the X-ray imaging process is based on the paraxial approximation in scalar wave field theory [24]. This especially requires that the propagation distances are much larger than the wavelength and that the optics and objects can be described by a thin-element transmission function. Both approximations are justified for the microscope arrangement described in the previous paragraph. Furthermore, quasimonochromatic object illumination conditions are assumed. Our calculations follow a model introduced in Ref. [25] for the theoretical investigation of visible-light differential interference contrast microscopy.

3.1. Image formation process

Our model for the microscope starts with the illumination system. The condenser is approximated as a secondary incoherent source consisting of a finite number of source points n. The source points are individually coherent but mutually incoherent. The criterion for this approximation to be valid, $\rho_{\mathrm{source}} \gg \rho_{\mathrm{airy}}$, is sufficiently fulfilled. ρ_{source} is the laser-plasma source image size generated by the condenser in the object plane and ρ_{airy} is the size of the

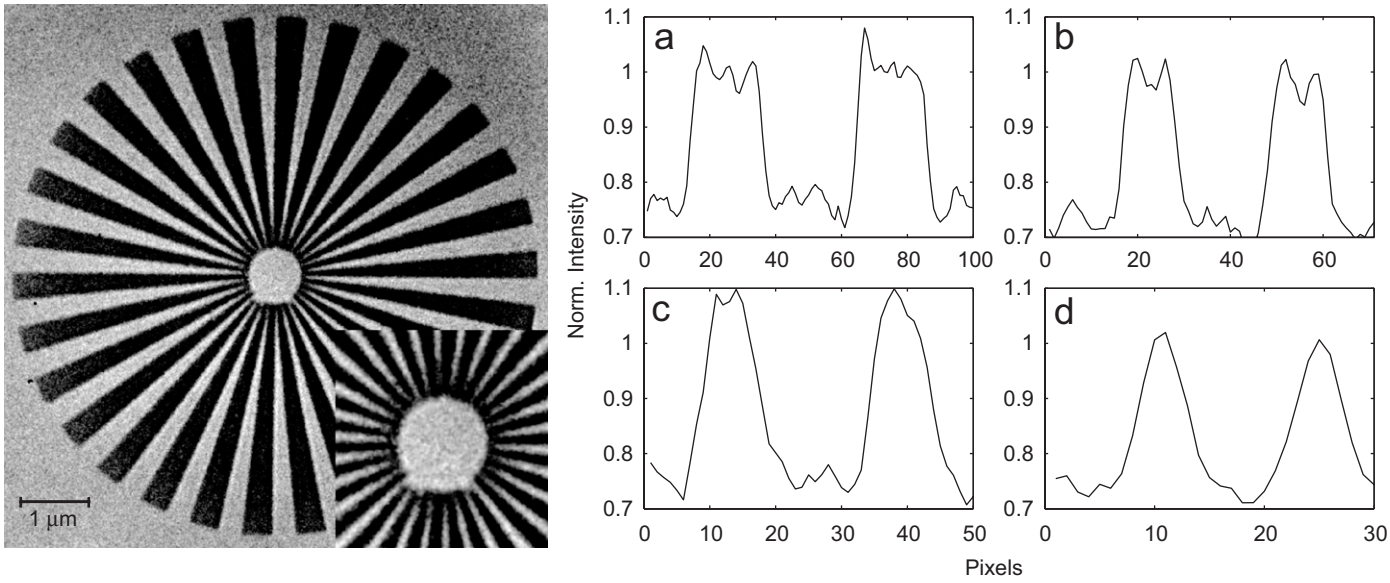

Fig. 2. Image of a Siemens star test object taken with the compact soft X-ray microscope. The inset shows the central part of the object with structure sizes down to 40 nm lines and spaces. Intensity profiles taken at different radial positions are shown as line plots to the right. The line plots are taken at radii of a—3 μm, b—2 μm, c—1.5 μm, and d—0.8 μm.

airy pattern as it would be created by a point-like laser-plasma source [26].

Each source point on the condenser emits a spherical wave, which in the object plane can be approximated by a plane wave at an angle. The plane wave field illuminates the object yielding the wave field directly behind the object as

$$U_{\text{object}}(x_0, y_0) = \psi_c(x_0, y_0) t(x_0, y_0), \tag{3.1}$$

$t(x_0,y_0)$ is the complex transmission function of the object and $\psi_c(x_0,y_0)$ is the illuminating plane wave field given by

$$\psi_c(x_0,\ y_0) = \frac{1}{\mathrm{i}\lambda z_c} \exp\left[\mathrm{i}\left(2\pi/\lambda\right)(x_0 \sin\theta_{xz} + y_0 \sin\theta_{yz})\right],$$

$$\tan\theta_{xz} = \frac{\eta}{z_c}, \quad \tan\theta_{yz} = \frac{\xi}{z_c}. \tag{3.2}$$

The coordinates are given in correspondence with Fig. 1, λ is the illumination wavelength and z_c is the distance between condenser and object plane.

The complex amplitude $U_{\text{object}}(x_0,y_0)$ is now used in coherent image formation, convolving it with the amplitude point-spread function (PSF) of the objective to yield the point source image [27]. The PSF for a diffractive zone plate can be calculated by propagating a wave field from an intensity point source through the optic to the image plane. This was tested to give identical results as for the diffraction-limited PSF of a normal lens, which can be calculated as the Fourier transform $\Im$ of the lens aperture, in this case a circular pupil function $P(x_0,y_0)$,

$$\mathrm{PSF}(u, v) = \Im\{P(x_0, y_0)\}. \tag{3.3}$$

The pupil function is defined as one on the zone plate and zero outside. The PSF is convolved with the complex amplitude of the illuminated object to yield the image intensity from a given point on the condenser,

$$I_{\text{image}}(u, v) = \left|U_{\text{image}}(u, v)\right|^2 = \left|\mathrm{PSF}(u, v) \otimes U_{\text{object}}(\tilde{x}_0, \tilde{y}_0)\right|^2 \tag{3.4}$$

The illuminated object function is now given in reduced coordinates, taking into account the magnification of the optical system, and $\otimes$ denotes a convolution.

The image intensity for each point on the condenser is calculated accordingly and the final image is obtained by adding up all n images.

$$I_{\text{image}}(u, v) = \sum_n \left|\mathrm{PSF}(u, v) \otimes U_{\text{object}}(\tilde{x}_0, \tilde{y}_0)\right|^2 \tag{3.5}$$

Note that the corresponding image intensities for the cases of coherent and incoherent illumination are given by

$$I_{\text{image}}(u, v) = \left|\mathrm{PSF}(u, v) \otimes t(\tilde{x}_0, \tilde{y}_0)\right|^2 \tag{3.6}$$

$$I_{\text{image}}(u, v) = \left|\mathrm{PSF}(u, v)\right|^2 \otimes \left|t(\tilde{x}_0, \tilde{y}_0)\right|^2 \tag{3.7}$$

respectively. These are two linear relationships between image and object, while for partially coherent image formation the relation is non-linear.

3.2. Numerical implementation

The image formation calculations were implemented using a Matlab code and were carried out on an AMD Opteron 2.8 GHz dual processor computer with 16 GB of RAM. A 5000×5000 matrix was used together with a pixel size of 2 nm in order to resolve the plane wave field at the object. The convolution in Eq. (3.4) is carried out as a multiplication in Fourier space. A total of 100 source points were placed on the inner and outer rim of the condenser to approximate the incoherent secondary source. Finally, the image was reduced to an 800×800 matrix to correspond to the CCD detector pixel size of 13 μm. The total computation time using these parameters was 103 min for a complete two-dimensional image.

4. Results

Simulated images for the three types of illumination conditions are shown in Fig. 3. An enlarged section of the center of each image is shown on the inset as well as the intensity line plots to the right. By studying the line plots, clear distinctions between the three cases can be made. The incoherent case (lower right) illustrates the nickel absorption of 34% (corresponding to the local thickness of 75 nm) with a fully resolved test object and typical intensity profiles in accordance with incoherent image formation. On the contrary, the coherent case (lower left) shows "ringings" or diffraction-like features in the line plots which are artifacts from the coherence conditions. The partially coherent case (top) is clearly a situation that can be described as being situated between the two previously described cases. The line plots display damped, but still existing, coherence artifacts. This indicates that the presently simulated image for partially coherent illumination is closer to the coherent limit than the incoherent, as predicted by the coherence factor m.

One can now compare the simulated images with the image from the microscope, shown in Fig. 2. Studying the line plots, qualitative agreements between the microscope image and the simulated image for partially coherent illumination are found. Since the simulation is not modeling microscope conditions like astigmatism, other aberrations and the non-homogenous illumination profile, there exists a quantitative disagreement between microscope image and simulated image. The discrepancy also results from uncertainties in the real object thickness, a slight drift of the object during exposure [4] as well as noise in the measured image. However, the model is sufficient in reproducing the main features visible in the images from the microscope.

5. Conclusion

The partially coherent object illumination with a coherence factor of $m = 0.3$ has an influence on the images obtained for a Siemens star test object in the BIOX

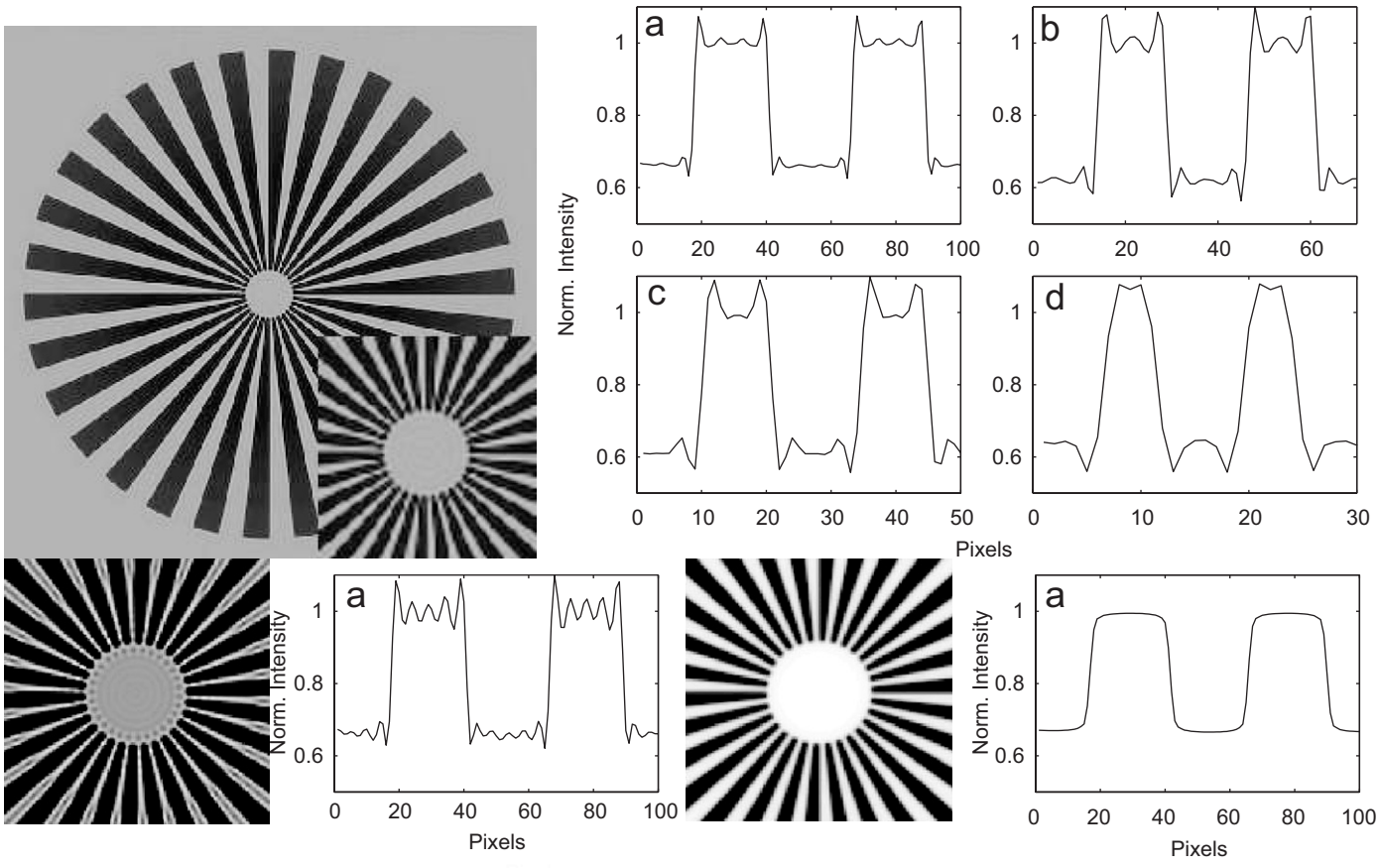

Fig. 3. The simulated images of the Siemens star object, with intensity line plots. The upper image is the partially coherent case ($m = 0.3$), the lower left the coherent ($m = 0$) and the lower right the incoherent one ($m \to \infty$). Again, the line plots are taken at radii of a—3 μm, b—2 μm, c—1.5 μm and d—0.8 μm.

compact soft X-ray transmission microscope. Using an image formation model including partial coherence it was shown that diffraction-like edge effects are a direct consequence of the illumination conditions. The imaging model developed is relatively simple and can easily be implemented numerically.

Further improvements of the model will take into account zone plate aberrations like astigmatism as well as defocusing. Another interesting application of the model is the simulation of X-ray differential interference contrast microscopy using special diffractive optical elements as objective optics [28,29]. In general, the simulation will help to understand more about the image formation process in compact X-ray microscopes. It has to be noted that the model applies for synchrotron-based instruments as well, given that the condenser can be approximated as a secondary incoherent source.

For the future development of the compact microscope instrument, the simulation indicates that it is desirable to work with a condenser in which the numerical aperture is better matched to the objective one. However, using the microscope for imaging of not only artificial test samples with sharp edges but relevant objects, it remains to be seen if the actual illumination conditions have a negative effect on the images or not.

Acknowledgements

This project was supported by the Swedish Science Research Council and the Swedish Strategic Research Foundation. The authors would like to thank Hans Hertz and Göran Manneberg for helpful discussions.

References

[1] S. Aoki, Y. Kagoshima, Y. Suzuki (Eds.), X-ray Microscopy, IPAP Conference Series 7, Tokyo, 2006.
[2] C.A. Larabell, M.A. Le Gros, Mol. Biol. Cell 15 (2004) 957.
[3] J. Thieme, G. Schneider, C. Knöchel, Micron 34 (2003) 339.
[4] P.A.C. Takman, H. Stollberg, G.A. Johansson, A. Holmberg, M. Lindblom, H.M. Hertz, submitted for publication. J. Microsc.
[5] M. Berglund, L. Rymell, M. Peuker, T. Wilhein, H.M. Hertz, J. Microsc. 197 (2000) 268.
[6] M. Hoshino, S. Aoki, Jpn. J. App. Phys. 45 (2006) 989.
[7] K. Woo Kim, et al., Phys. Med. Biol. 51 (2006) N99.
[8] J.W Goodman, Introduction to Fourier Optics, McGraw-Hill, New York, 1996, pp. 101–114.
[9] J.W Goodman, Statistical Optics, Wiley, New York, 1985, p. 198.

[10] K.K.H. Toh, Two-Dimensional Images with Effects of Lens Aberrations in Optical Lithography, EECS Department, UC, Berkeley, 1988.
[11] K.K.H. Toh, A.R. Neureuther, Proc. SPIE 772 (1987) 202.
[12] L. Jochum, W. Meyer-Ilse, Appl. Opt. 34 (1995) 4944.
[13] J.M. Heck, D.T. Attwood, W. Meyer-Ilse, E.H. Andersen, J. X-ray Sci. Technol. 8 (1998) 95.
[14] W. Chao, B.D. Harteneck, J.A. Liddle, E.H. Anderson, D.T. Attwood, Nature 435 (2005) 1210.
[15] S. Vogt, H.N. Chapman, C. Jacobsen, R. Medenwaldt, Ultramicroscopy 87 (2000) 25.
[16] G. Schneider, Ultramicroscopy 75 (1998) 85.
[17] P.A.C. Jansson, U. Vogt, H.M. Hertz, Rev. Sci. Instrum. 76 (2005) 43503–43515.
[18] M. Born, E. Wolf, Principles of Optics, Cambridge University Press, Cambridge, 1980, pp. 522–524.
[19] S. Rehbein, A. Holmberg, G.A. Johansson, P.A.C. Jansson, H.M. Hertz, JVST B 22 (2004) 1118.
[20] T. Wilhein, D. Hambach, B. Niemann, M. Berglund, L. Rymell, H.M. Hertz, Appl. Phys. Lett. 71 (1997) 190.
[21] A. Holmberg, S. Rehbein, H.M. Hertz, Microelectron. Eng. 73–74 (2004) 639.
[22] G.A. Johansson, A. Holmberg, H.M. Hertz, M. Berglund, Rev. Sci. Instrum. 73 (2002) 1193.
[23] M. Born, E. Wolf, Principles of Optics, Cambridge University Press, Cambridge, 1980, p. 523.
[24] J.W Goodman, Introduction to Fourier Optics, McGraw-Hill, New York, 1996, pp. 32–63.
[25] C. Preza, D.L. Snyder, J.-A. Conchello, J. Opt. Soc. Am. 16 (1999) 2185.
[26] M. Born, E. Wolf, Principles of Optics, Cambridge University Press, Cambridge, 1980, p. 520.
[27] J.W Goodman, Introduction to Fourier Optics, McGraw-Hill, New York, 1996, p. 133.
[28] U. Vogt, M. Lindblom, P.A.C. Jansson, T. Tuohimaa, A. Holmberg, H.M. Hertz, Opt. Lett. 30 (2005) 2167.
[29] C. Chang, A. Sakdinawat, P. Fischer, E. Anderson, D. Attwood, Opt. Lett. 31 (2006) 1564.